Original

REFLECTOR ANTENNAS - AN OVERVIEW OF SURFACE DISTORTION EFFECTS

Knud Pontoppidan
TICRA A/S
Kronprinsensgade 13
DK-1114 Copenhagen K

Telephone: +45 1 12 45 72, Telefax +45 1 12 08 80

ABSTRACT

Reflector antenna surface distortions may be slowly varying, rapidly varying, systematic or random. Typical examples of each of these types of surface distortions are presented and their consequences on the peak gain and side lobe performance are illustrated. It is demonstrated that the impact on the radiation pattern is strongly dependent on the type of surface distortion.

RESUME

Les distorsions de surface des antennes à réflecteur peuvent être: erreurs à variation lente, erreurs à variation rapide, systématiques ou aléatoires. Chacune de ces catégories est présentée à l'aide d'un exemple typique et les effets des erreurs sur le gain du faisceau principal ainsi que sur la qualité des lobes latéraux sont illustrés. Il est démontré que l'effet sur le diagramme de rayonnement est étroitement lié à la catégorie de distorsion.

1 INTRODUCTION

The use of higher frequencies and larger antennas makes it very important to be able to establish realistic requirements to the accuracy of the reflector antenna surface. The purpose of the present paper is to illustrate how different surface deformations influence the electrical characteristics of a reflector antenna.

2 CLASSIFICATION OF REFLECTOR SURFACE DISTORTIONS

It is in general desirable that the reflector surface is a paraboloid with focal point at the feed phase centre. In practice, the surface may deviate from this ideal shape for several reasons and it is convenient to subdivide the surface deviations in the following types,

a) deviations which change the desired paraboloid into another best fit paraboloid

b) slowly varying errors

c) rapidly varying errors

since the impact on the radiation field is very different from one group to the other.

All three types of surface deviations will often appear at the same time. This is illustrated in Figure 1, where, as an example, the actual shape is shown as a superposition of a best fit paraboloid, slowly varying systematic errors and rapidly varying random errors.

The errors, which give rise to the best fit paraboloid, could be due to thermal distortions, aging, residual stresses and other slowly varying distortions. If no other errors are present, this will give rise only to a tilt of the beam, but the peak gain, the side lobes and the cross polarization are - for realistic deformations - practically unchanged.

It is convenient also to distinguish between systematic errors and random errors. Systematic errors are surface deviations which are inherent in the construction of the antenna and which are predictable, whereas random errors are unpredictable but within some given statistical limits.

Systematic errors may be slowly or rapidly varying across the reflector surface. An example of slowly varying systematic errors are thermal distortions. Rapidly varying systematic surface deviations appear for unfurlable reflectors, where the mesh is fixed at given intervals.

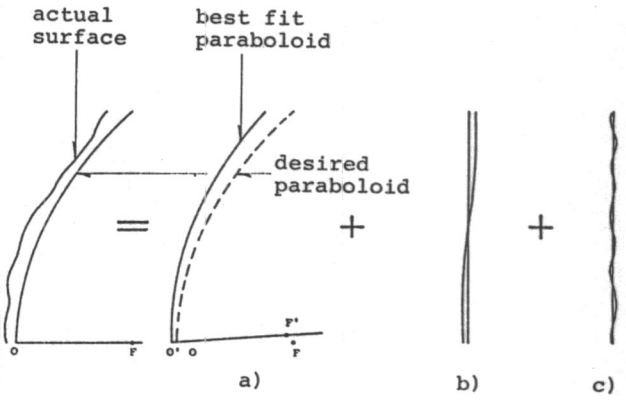

Figure 1 Subdivision of surface errors
a) best fit paraboloid
b) slowly varying
c) rapidly varying

Random errors are typically caused by the fabrication tolerances in the manufacturing process. The distinction between systematic and random errors may be fluid. It may be convenient, for example, to consider thermal distortions as a random slowly varying error in a parametric investigation in order to establish the acceptable thermal distortion levels. However, once an antenna design has been fixed and the construction selected, the thermal distortions are systematic errors that can be predicted, and the influence on the RF-performance can be accurately determined.

The influence on the RF-performance for the different types of surface distortions is described in the following.

It is important to note that when the total rms surface error is less than about 0.05λ (λ = wavelength) all effects are linear. This means that the total field may be calculated by a direct summation, in amplitude and phase, of the undistorted pattern and individual error fields calculated separately.

3 SLOWLY VARYING DISTORTIONS

For a general investigation of slowly varying distortions it is convenient to be able to generate such surfaces in a systematic manner. This can be done by superimposing a square grid on the undistorted reflector surface, as shown in Figure 2. The node values are selected as random numbers uniformly distributed in a given interval (the peak-to-peak value) and with a mean value equal to zero. An interpolation function yields a smooth surface between the random values at the nodes. The spacing between the nodes, c, relative to the reflector diameter, D, determines the roughness of the surface. This is illustrated in Figure 3 which shows surface distortions for c/D = 0.4, 0.2, 0.1 and 0.05. The correlation distance is 2c, meaning that within a circular area of diameter 2c the surface distortions are correlated, whereas they are completely uncorrelated for larger distances.

It is seen from Figure 3 that typical thermal distortions correspond to relatively large values of c/D, say between 0.2 and 0.4. The surface shape for c/D = 0.05 is more typical for the uncertainties related to manufacturing tolerances.

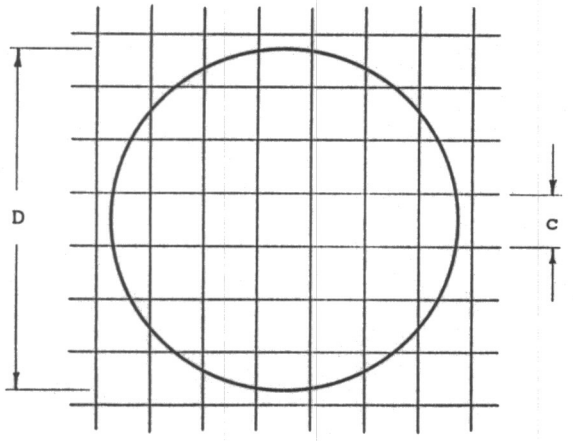

Figure 2 Grid for reflector distortion definition

The slowly varying surface distortions will often turn out to generate the most important RF degradations because they affect the radiation pattern near the main beam and the very first sidelobes. Therefore, the slowly varying surface distortions have been investigated in detail and an analysis approach has been developed. The idea of this analysis method is to expand the surface distortions in a series of Zernike polynomials. For each of the modes in this expansion the influence on the far field pattern is known. It is therefore possible to evaluate the impact of a particular distortion directly from the Zernike mode expansion.

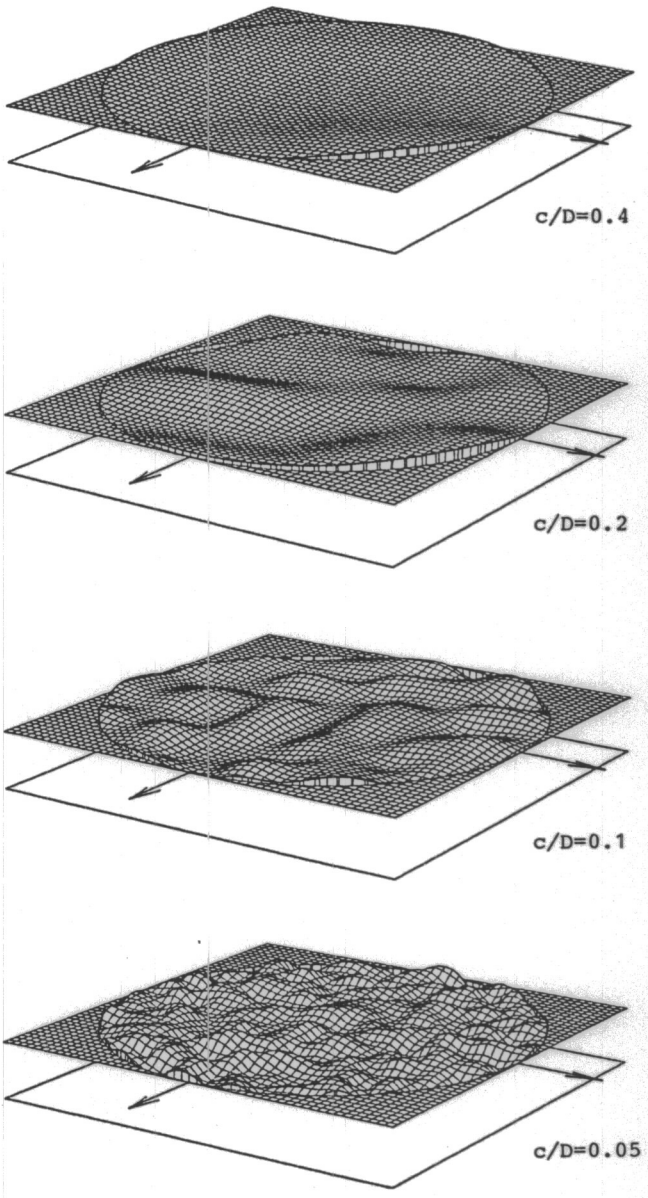

Figure 3 Surface distortions for different values of c/D.

3.1 Zernike mode approach

The Zernike polynomials are used in optics for the investigation of aberrations (see e.g. Born and Wolf, 1983). They have also been applied to model the aperture phase of a single feed contoured beam reflector antenna (Jørgensen, 1983).

The Zernike polynomials are in general complex valued functions. In the present context we are interested in the real part only and each mode may then be written

$$Z_n^m(x,y) = R_n^m(\rho)\cos(m(\phi - \phi_n^m)) \qquad (1)$$

where ϕ_n^m is a reference direction. The radial function $R_n^m(\rho)$ is a polynomium in ρ containing the powers $\rho^m, \rho^{m+2}, \ldots, \rho^n$. The Zernike polynomials are orthogonal over the unit circle.

The polynomials $R_n^m(\rho)$ are listed in Table 1 for $m \leq 8$ and $n \leq 8$ (from Ref. 4). The functions are normalized such that $R_n^m(1) = 1$.

The Zernike polynomials are characteristic by the fact that they are not only polynomials for the radial dependence $R_n^m(\rho)$ but they are also polynomials in x and y.

The modes m = n = 1 and m = 0, n = 2 represent a plane and a paraboloid, respectively. The modes for which m + n = 4 are the primary aberrations in optical systems:

m = 0, n = 4: spherical aberration
m = 1, n = 3: coma
m = 2, n = 2: astigmatism

Three-dimensional plots of some of the Zernike polynomials are shown in Figure 4.

The orthogonality of the Zernike modes is used to determine the coefficients, σ_n^m, in the expansion of a distorted surface. A computer program for this purpose has been developed and it has been used to expand the distortions exemplified in Figure 3 for d/D = 0.2. The result is shown in Figure 5 for modes up to $m \leq n \leq 20$. The sizes of the shaded areas represent the relative amplitude of a particular mode.

It is seen from Figure 5 that only the modes up to about m = n = 14 are necessary for representing this distortion example. The mode m = n = 1 will generate a beam tilt and can be removed by a lateral displacement of the feed. Similarly, the (m,n) = (0,2) can be removed by an axial displacement of the feed. The coefficients to these modes can therefore be used to determine the optimum feed position for the actual reflector shape (the best fit paraboloid).

The error signal generated by one Zernike mode may for uniform aperture illumination be written as

$$E_e = \delta_n^m j^{(m+1)} \frac{J_{n+1}(ka\sin\theta)}{ka\sin\theta}\cos(m(\phi - \phi_n^m)) \qquad (2)$$

apart from constant factors. δ_n^m is the amplitude of the distortion mode, $k = 2\pi/\lambda$ and a = D/2. This expression for the distortion field exhibits several interesting characteristics. The factor $j^{(m+1)}$ implies that the distortion field for all odd m will be in phase with the undistorted pattern and therefore the influence on the sidelobe levels will be much more pronounced than for even values of m. The azimuthal variation, $\cos m\phi$, is, as expected, identical to that of the surface error itself. The amplitude of the distortion field is controlled by the factor $J_{n+1}(ka\sin\theta)/ka\sin\theta$ and it is independent of m. Figure 6 shows the angular variation of the distortion field for n = 4, 8, 12, 16 and 20 where the amplitude of the distortion is $\delta_n^m = 0.01\lambda$. For comparison also the undistorted pattern is shown in Figure 6.

It is seen, that the maximum influence of the distortion moves away from the main beam as the mode number is increased and for values of the argument lower than the maximum, the function decays very rapidly and its influence on the pattern will be practically negligible.

The present analysis is aimed at slowly varying surface errors which concentrate at the main beam and the first few sidelobes. Figure 6 shows that if effects outside the third sidelobe are ignored, only modes up to about 12 in m and n need be considered.

In the case of a tapered illumination of the aperture the distortion field cannot be expressed by a simple formula. The distortion field can, however, very well be evaluated numerically by a one-dimensional integral in the radial direction and the general characteristics remain unchanged.

The above expression (2) includes only first order effects of the distortions. The consequence of this is that all distortion effects vanish in the boresight direction, $\theta = 0$. For uniform illumination it is possible to include also the second order effect which will give the correct variation near $\theta = 0$ including the well-known axial gain decrease, $\exp((-4\pi\varepsilon_{rms}/\lambda)^2)$, ε_{rms} being the rms value of the surface distortions. This limitation for tapered illuminations does not jeopardize the practicability of the method since the second order effects are only significant near the main beam peak and the axial gain drop is known anyway from the ε_{rms} value of the surface distortions.

The total field from the antenna is determined by combining the field from the undistorted antenna with the modal error fields described above. The total field is calculated by a direct summation, in amplitude and phase, of the undistorted pattern and all the modal error fields weighted by the individual amplitudes. The number of modes necessary in the expansion depends on the angular region of interest.

The radiation pattern for an antenna with diameter $D = 41.5\lambda$ and with the surface distortion in Figure 3 for d/D = 0.2 is shown in Figure 7. It is seen that the slow variation of the surface distortion limits the RF degradations to the main beam and the first couple of side lobes. It should be noted that the nominal pattern is rotationally symmetric but the distortion field is not. This is illustrated in Figure 8 which shows a contour plot of the distortion field. The lack of symmetry means that the influence of the distortions may be very different in different pattern cuts and there may be pattern cuts where the distortion effects are practically invisible (along the dotted line in Figure 8)

m \ n	0	1	2	3	4	5	6	7	8
0	1		$2\rho^2-1$		$6\rho^4-6\rho^2+1$		$20\rho^6-30\rho^4+12\rho^2-1$		$70\rho^8-140\rho^6+90\rho^4-20\rho^2+1$
1		ρ		$3\rho^3-2\rho$		$10\rho^5-12\rho^3+3\rho$		$35\rho^7-60\rho^5+30\rho^3-4\rho$	
2			ρ^2		$4\rho^4-3\rho^2$		$15\rho^6-20\rho^4+6\rho^2$		$56\rho^8-105\rho^6+60\rho^4-10\rho^2$
3				ρ^3		$5\rho^5-4\rho^3$		$21\rho^7-30\rho^5+10\rho^3$	
4					ρ^4		$6\rho^6-5\rho^4$		$28\rho^8-42\rho^6+15\rho^4$
5						ρ^5		$7\rho^7-6\rho^5$	
6							ρ^6		$8\rho^8-7\rho^6$
7								ρ^7	
8									ρ^8

Table 1 The radial polynomials $R_n^m(\rho)$ for $m < 8$ and $n < 8$
(from Born and Wolf (1983))

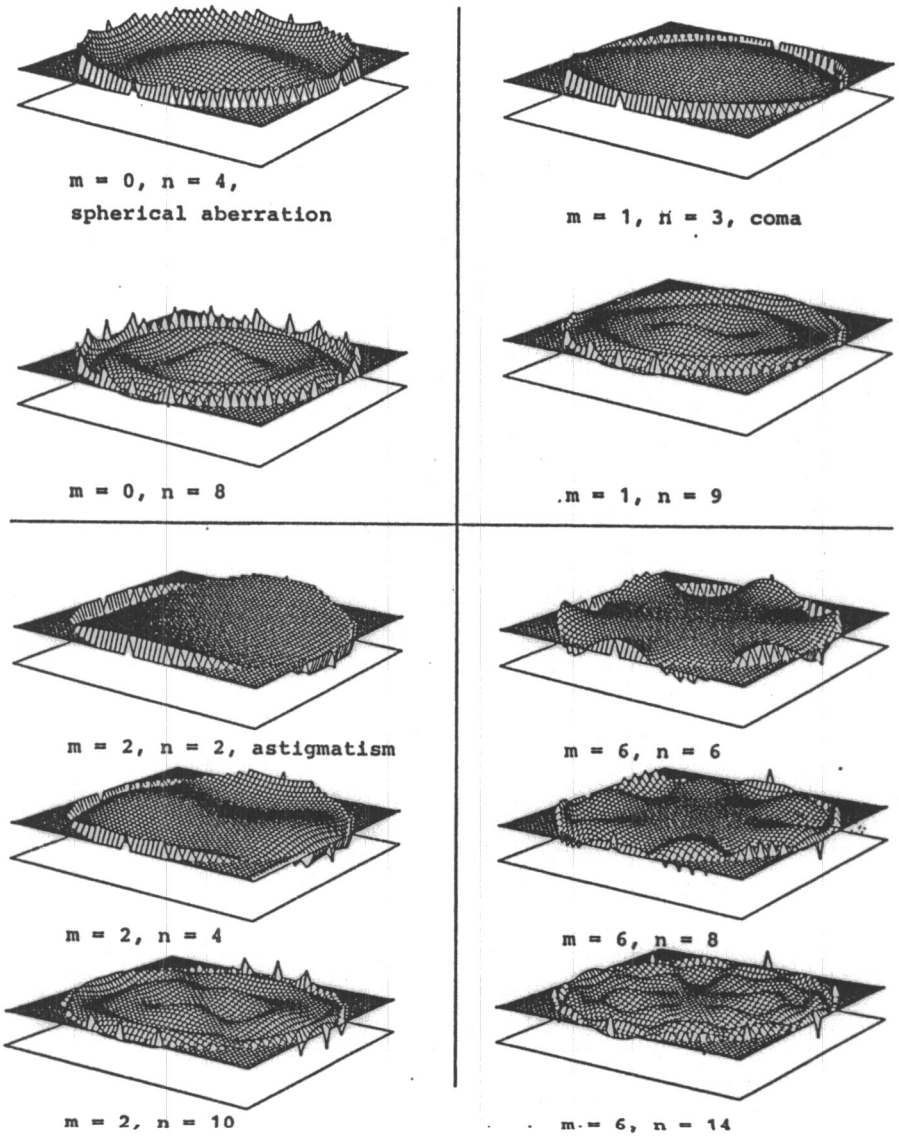

Figure 4 Samples of Zernike modes for surface representation

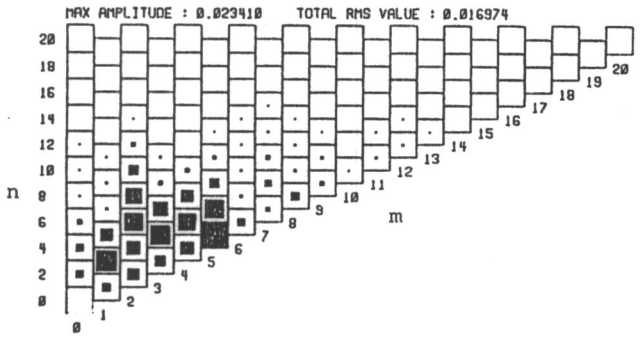

Figure 5 Relative amplitudes of expansion coefficients for the surface distortion in Figure 3, c/D = 0.2

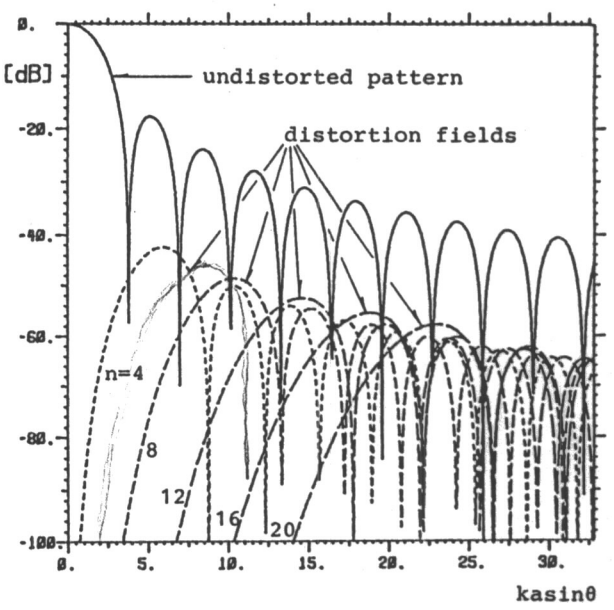

Figure 6 RF distortion fields for modal surface distortions with peak error 0.01λ
n = 4,8,12,16,20
uniform illumination

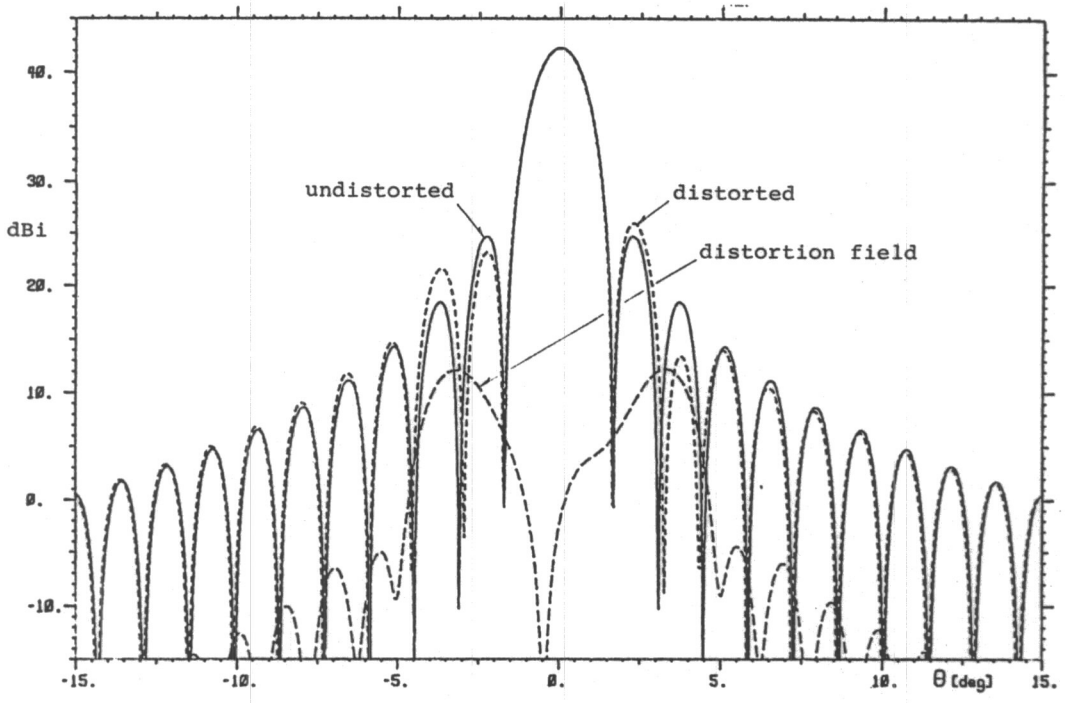

Figure 7 Radiation pattern for reflector antenna,
D = 41.5λ,
Slowly varying surface distortion (Figure 3, c/D = 0.2)
uniform illumination

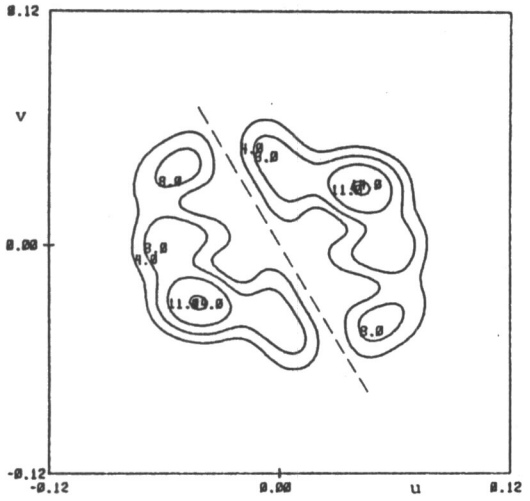

Figure 8 Amplitude of the distortion field, levels in dBi

3.2 Applicational example

The Zernike mode approach will be illustrated by a realistic example, namely an inflatable antenna developed by Contraves, Switzerland, as separately described by Hammer, Pagana and Bermascoui (1986) in another paper at this conference.

A photograph of the inflated antenna is shown in Figure 9. The focal length of the parent offset paraboloid is 2.33 m and aperture diameter is 2.81 m. The reflector surface shape has been measured mechanically by Contraves and x-, y- and z-coordinates to about 600 surface points have been made available to TICRA.

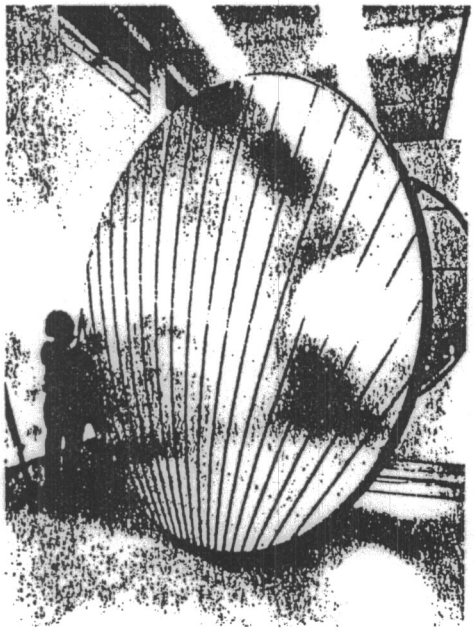

Figure 9 The Contraves inflatable antenna

For the RF calculations to be presented in the following it has been assumed that the feed radiates a balanced pattern with phase center at the focus of the parent paraboloid and providing a 20 dB edge taper. The feed is linearly polarized in the plane of symmetry. The frequency is 3.63 GHz.

For all analyses of reflector surfaces it is very desirable that the reflector surface data points are available in a regular xy-grid. This is often not the case if the surface data are the results of a direct measurement or the output of a mechanical finite element calculation.

The method adopted here to obtain the regular grid has been described by Akima (1978). The input points - which may be completely arbitrarily distributed - are automatically connected to form the "best" possible triangular grid. Interpolation functions within each triangle will yield a continuous and smooth surface and are used to calculate the surface points in the regular grid.

The measured input points and the triangular grid for the Contraves antenna is shown in Figure 10. Once the data points have been transformed to a regular grid they can be used for further analyses and they can be represented visually as shown by the 3D-plot in Figure 11. Two types of surface errors are clearly identified. Slowly varying distortions - which perhaps are due to unequal tensions in the membrane material - are superimposed by minor rapidly varying errors along the intersections between the gore sections.

The Zernike mode expansion for the surface distortions in Figure 11 are shown in Figure 12. It is seen that the rapid variations on the reflector surface give rise to many Zernike modes of high order and small amplitude. However, only the dominant lower order modes will affect the radiation pattern near the main beam and the first sidelobes. Figure 13 shows the surface distortions generated by the Zernike mode expansion including only the modes up to $m < n < 12$.

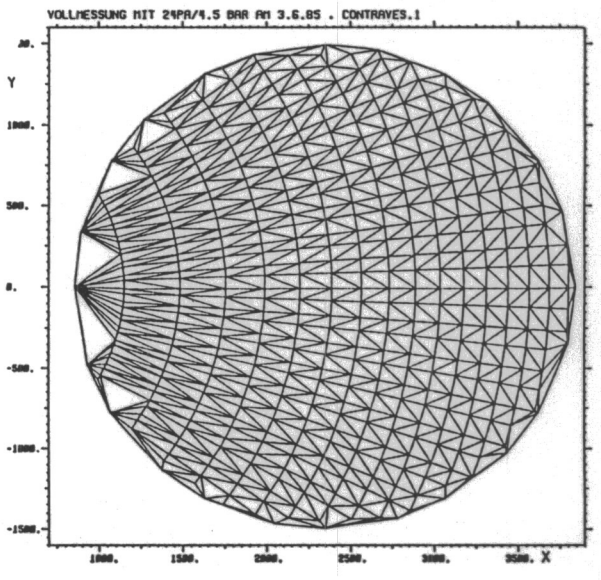

Figure 10 Contraves inflatable antenna
Measured points and triangularization

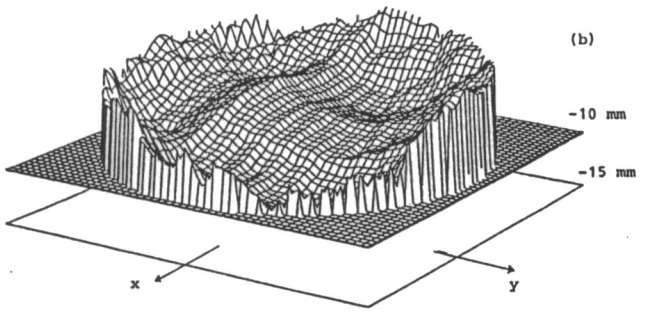

Figure 11 Contraves inflatable antenna
Deviations from parent paraboloid

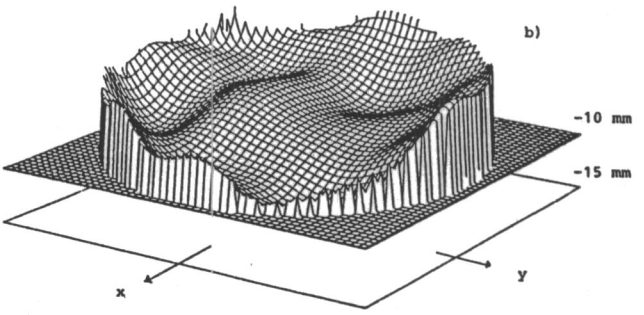

Figure 13 Contraves inflatable antenna
Surface deviations from parent paraboloid represented by Zernike modes up to
$m \leq n \leq 12$

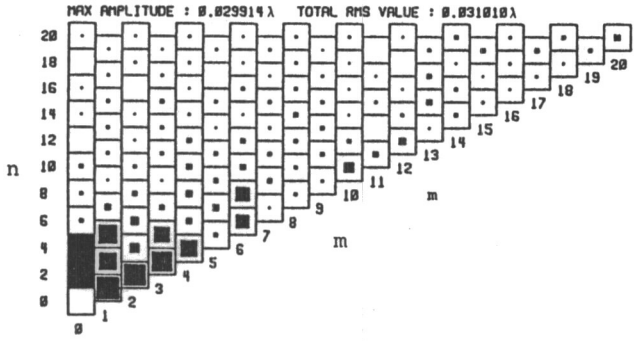

Figure 12 Contraves inflatable antenna. Relative amplitudes of surface expansion coefficients.

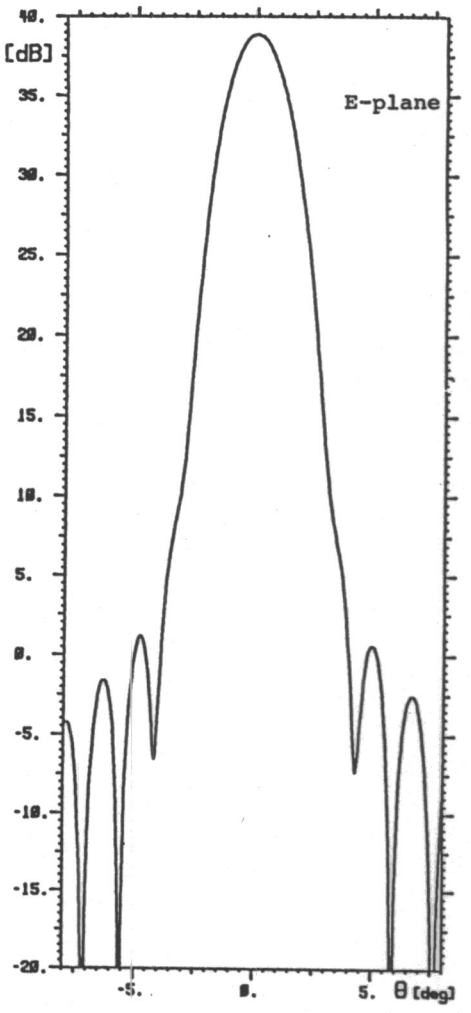

Figure 14 E-plane radiation pattern for the ideal Contraves antenna.

For the Contraves inflatable antenna the rms surface error is about 1.3 mm which corresponds to 0.016λ. The validity of superposition is therefore satisfied.

The Zernike mode approach for evaluating surface distortions will now be compared to a rigourous Physical Optics analysis (GRASP).

The E-plane radiation pattern for the undistorted antenna (ideal paraboloid) is shown in Figure 14 in a region ±8 degrees from boresight.

The pattern calculated by GRASP for the actually realized surface is shown in Figure 15. The surface is here represented by the measured data transformed into a regular grid as shown in Figure 11. It is seen that the distortions have a significant impact on the patterns, especially the sidelobes which are increased by up to 10 dB.

Figure 15 also shows the pattern obtained by the Zernike mode approach, i.e. adding the individual distortion patterns to the undistorted pattern in Figure 14. It is seen that the accuracy is very good and certainly adequate for the proposed application. In Figure 15 only the modes up to $m \leq n \leq 12$ are included. Higher order modes would only radiate for $\theta > 8.5$ degrees, i.e. outside the pattern range in Figure 15.

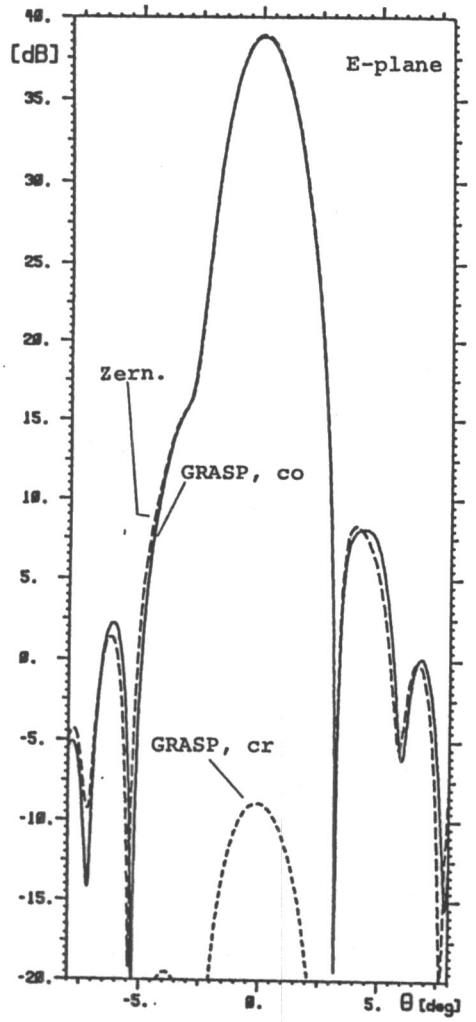

Figure 15 E-plane radial pattern for the Contraves antenna with the realized surface.
GRASP solution with measured reflector surface (Figure 11).
Zernike solution with modes up to $m < n < 12$.

The main advantage of the proposed analysis method is - apart from computer time - that there is a close relation between a given type of surface deformation and the impact on the radiation pattern. This makes it possible by simple means to determine how the reflector construction should be changed in order to improve the performance.
Rapid surface distortions, which generate modes of high order, will contribute only in the far-out side lobe region. If the region of interest is limited to the main beam and the first few side lobes, only the lower order modes need be determined. Consequently, only a limited number of input points are necessary. For the Contraves antenna described above the distortion effects would have been adequately predicted with about 100 uniformly distributed points.

4 RAPIDLY VARYING DISTORTIONS

In this section the effects of rapidly varying surface distortions will be described. They will be divided in systematic errors resulting from the construction of the antenna and random errors caused by the manufacturing tolerances.

4.1 Systematic distortions

The systematic surface distortion will be illustrated by two types of unfurlable reflector antennas, the umbrella concept and the 3D-scissors concept. In the umbrella design the reflecting mesh is attached continuously along the supporting parabolic ribs, whereas in the 3D-scissors design the mesh is fixed to the nodes of a regular triangular lattice, see Figure 16. The actual shape of the reflecting mesh will derivate from the desired paraboloidal form, as illustrated in Figure 17.

The gore sectors of the umbrella antenna will give rise to increased side lobes, the so-called gore lobes. The gore lobes do not affect the pattern near the main beam and the first side lobes, but they appear from an angle given approximately by

$$\sin \theta_g = \frac{N_g}{\pi \, D/\lambda} \qquad (3)$$

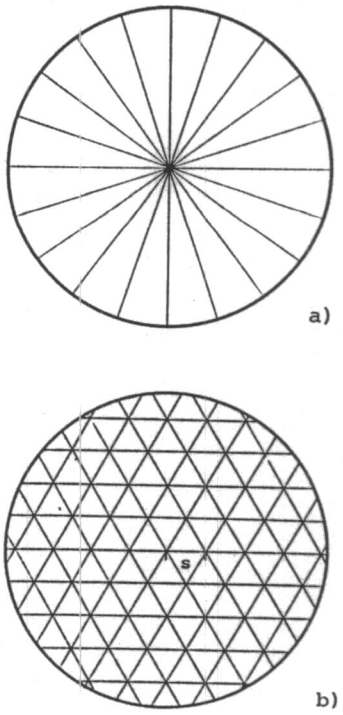

Figure 16 Construction principles of unfurlable antennas.
a) umbrella concept
b) 3D-scissors concept

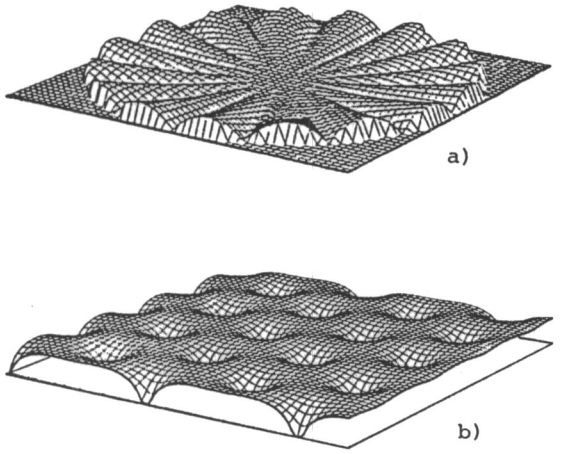

Figure 17 Surface deviations relative to parent paraboloid for
a) umbrella concept
b) 3D-scissors concept

where N_q is the number of ribs (or gores). The gore lobes are approximately rotationally symmetric around the main beam axis. The radiation pattern of an umbrella antenna with 20 ribs is shown in Figure 18b and the pattern for the undistorted paraboloid is shown in Figure 18a.

The two-dimensional periodic structure of the 3D-scissor surface gives rise to grating lobes. The angular position θ_{gr} of the grating lobes closest to the main beam is given by

$$\sin \theta_{gr} = \frac{2\lambda}{\sqrt{3}\, s} \qquad (4)$$

where s is the distance between the node points in the scissor construction.

The systematic nature of the surface distortions concentrates the energy in the grating lobes and, as for the umbrella antenna, the main beam and the inner side lobes are practically unaffected. Figure 18c shows the pattern where the grating lobes are clearly visible.

4.2 Random distortions

The random errors of a reflector antenna surface are typically associated with the manufacturing tolerances and with the finite accuracy of adjustment and measurement (e.g. unfurlable antennas) of the realized surface.

Random errors on the reflector surface will scatter the field from the forward direction into the sidelobe region thus reducing the peak gain and increasing the sidelobes. Random errors have been investigated by Ruze (1966). His classical results have proven to be very useful and are summarized below.

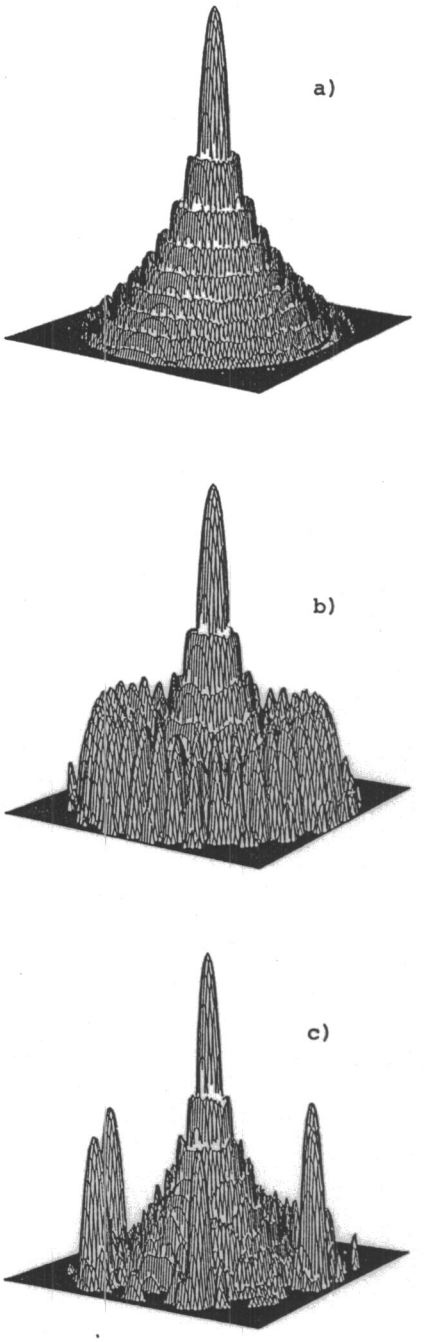

Figure 18 Radiation patterns for unfurlable antennas
a) nominal pattern
b) umbrella concept
c) 3D-scissors concept

The peak gain is reduced by the factor

$$e^{-(\frac{4\pi\varepsilon_{rms}}{\lambda})^2} \qquad (5)$$

where ε_{rms} is the root mean square surface error. This expression is with good approximation valid not only for random errors, but for any type of error measured relative to the best fit paraboloid.

The power pattern of the distortion field generated by the surface errors is - for small errors - given by

$$G_s = (\frac{2\pi c}{\lambda})^2 \, (\frac{4\pi\varepsilon_{rms}}{\lambda})^2 \, e^{-(\pi\sin\theta)^2(c/\lambda)^2} \qquad (6)$$

where 2c is the correlation distance of the surface errors and θ is the angular distance from boresight. The relation (6) is illustrated graphically in Figure 19 for $\varepsilon_{rms} = 0.01\lambda$. Note that the distortion pattern is independent of the size of the reflector, D/λ. The expression (6) is not valid near the axis ,$\theta = 0$, where instead expression (5) should be used.

Random surface distortions can be generated numerically by the approach illustrated in connection with Figure 2 where the distance c between the grid lines will result in a correlation distance of 2c.

In order to illustrate the range of applicability of Ruze's simple formulas the four surface distortion examples of Figure 3 will be investigated. Figure 20 shows for each value of c/D

- the grid used for generating the surface distortion
- the surface distortion shape (repeated from Figure 3)
- the Zernike mode expansion of the surface distortion, $\varepsilon_{rms} = 0.01\lambda$
- a pattern cut, $D = 41.5\lambda$, uniform illumination

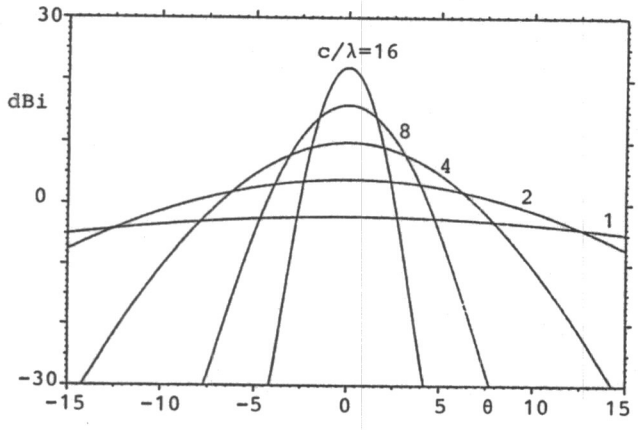

Figure 19 Distortion field for random surface error with rms value 0.01λ

The pattern cuts include the

- nominal field
- distorted field
- distortion field
- Ruze approximation (6) for the distortion field

The distortion field is the vectorial difference between the nominal field and the distorted field.

Although the values of c/D = 0.2 and 0.4 are more typical for slowly varying distortions they are included here to illustrate the dependence with surface roughness. Figure 20 shows that for these cases the surface shape is represented by a relatively small number of Zernike modes and the field can be calculated at any point by the approach described in Section 3.1.

For c/D = 0.1 and 0.05 the surface shape is so rapidly varying that the number of modes necessary for a Zernike mode expansion becomes too large for practical applications. Figure 20 shows that the distortion pattern becomes very broad such that the whole side-lobe region is affected. It is worthwhile to note that Ruze's formula, expression (6), gives a very good overall approximation to the distortion field (except near the axis). Expression (6) cannot be used to calculate the distorted pattern at a particular point since the phase is unknown. This is not a practical limitation since the requirement to manufacturing tolerances will be based on all side lobes remaining within acceptable limits.

For c/D = 0.05 the number of points used to define the random surface is about 300. This number is similar to the number of mesh fixation points of a realistic unfurlable antenna. The result in Figure 20 for c/D = 0.05 is therefore representative for the mesh adjustment errors of an unfurlable antenna.

5 CONCLUSIONS

It has been demonstrated that different types of surface distortions have very different impacts on the radiation performance. For a particular design it is therefore necessary to determine the types of reflector deformations that can appear, before the realistic requirements to the accuracy are established.

Slowly varying surface distortions, typically generated by thermal distortions, are efficiently dealt with by means of the Zernike mode approach. Each mode in the expansion of the surface distortion will give rise to a particular electrical distortion field. This relationship makes it possible to evaluate how a mechanical construction should be modified in order to reduce the RF degradations. It is especially important to point out that the effect of slowly varying surface errors is concentrated in the region of the first side lobes and therefore, these errors play a decisive role when dealing with antennas with stringent requirements to the side lobe performance.

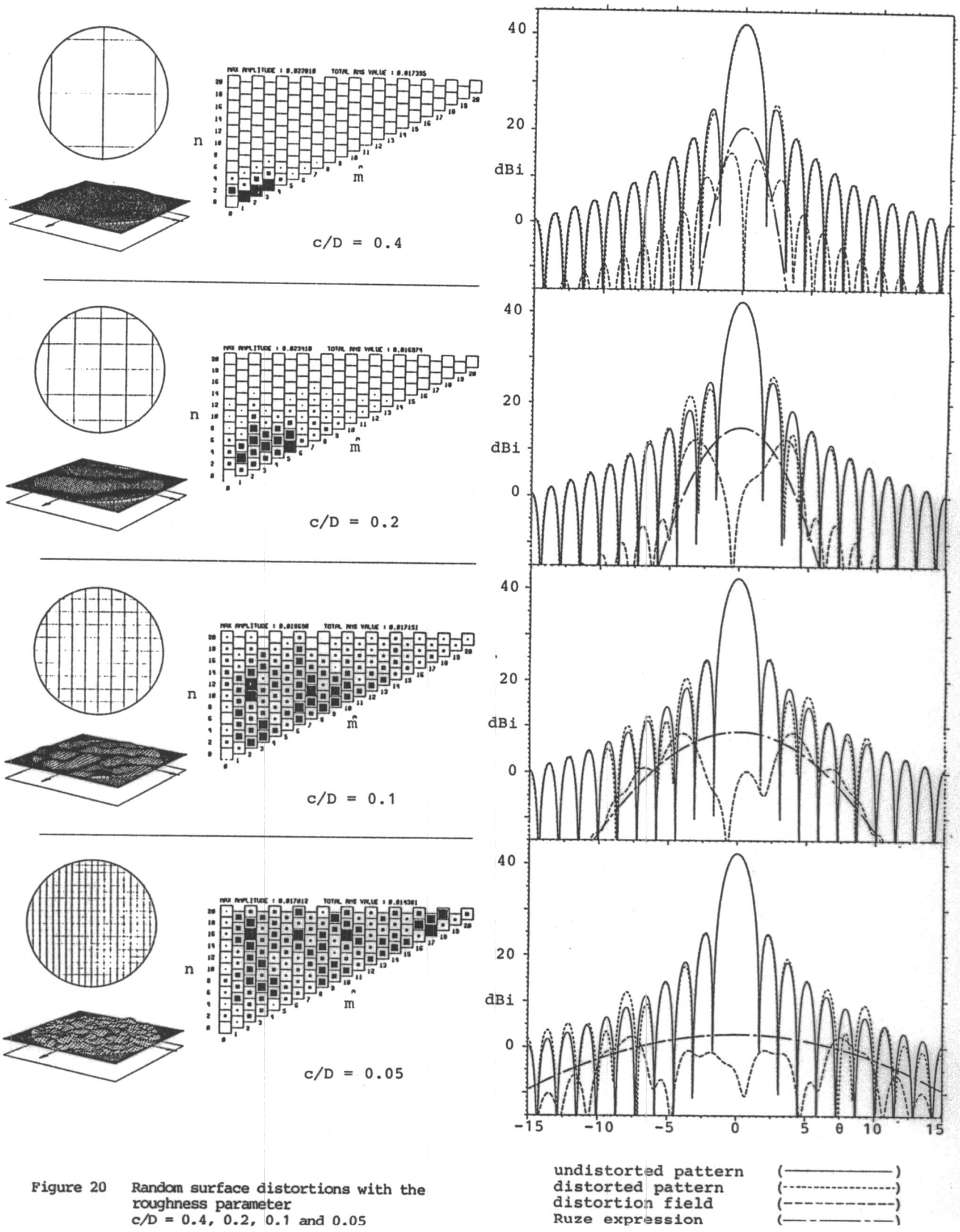

Figure 20 Random surface distortions with the roughness parameter
c/D = 0.4, 0.2, 0.1 and 0.05

Rapidly varying random errors due to manufacturing tolerances and limited adjustment accuracy are well described by statistical methods. In contrast, rapidly varying systematic surface errors, typical for unfurlable antennas or reflectors constructed by panels, give distinct effects (grating lobes) on the radiation pattern which will have to be calculated on a case by case basis.

6 REFERENCES

1. H. Akima (1978), "A method of bivariate interpolation and smooth surface fitting for irregularly distributed data points." ACM Trans. Math. Softw. 4, 2(June 1978), 148-159; also, Algorithm 526. ACM Trans. Math. Softw. 4,2(June 1978), 160-164.

2 H. Born and E. Wolf (1983), "Principles of optics", Sixth (corrected) edition, Pergamon Press.

3 J.A. Hammer, E. Pagana and M.C. Bernasconi (1986), "RF performance of the first 2.8m offset inflatable rigidized reflector", JINA 1986, Nice 4-6 Nov.

4. R. Jørgensen (1983), "Software support for optimization of contoured beam reflector antennas", volume 2: "Shaped Reflector antenna", Final report on ESTEC Contract 4967/82/NL/MS, TICRA report S-159-06.

5 J. Ruze (1966), "Antenna Tolerance Theory - A Review", Proc. IEEE, Vol 54, No 4, p 633-40.